Supporting Information

Artificial Intelligence Enabled Reagent-free Imaging Hematology Analyzer

Xin Shu, Sameera Sansare, Di Jin, Xiangxiang Zeng, Kai-Yu Tong, Rishikesh Pandey, Renjie Zhou**

1. Diffraction phase microscopy system

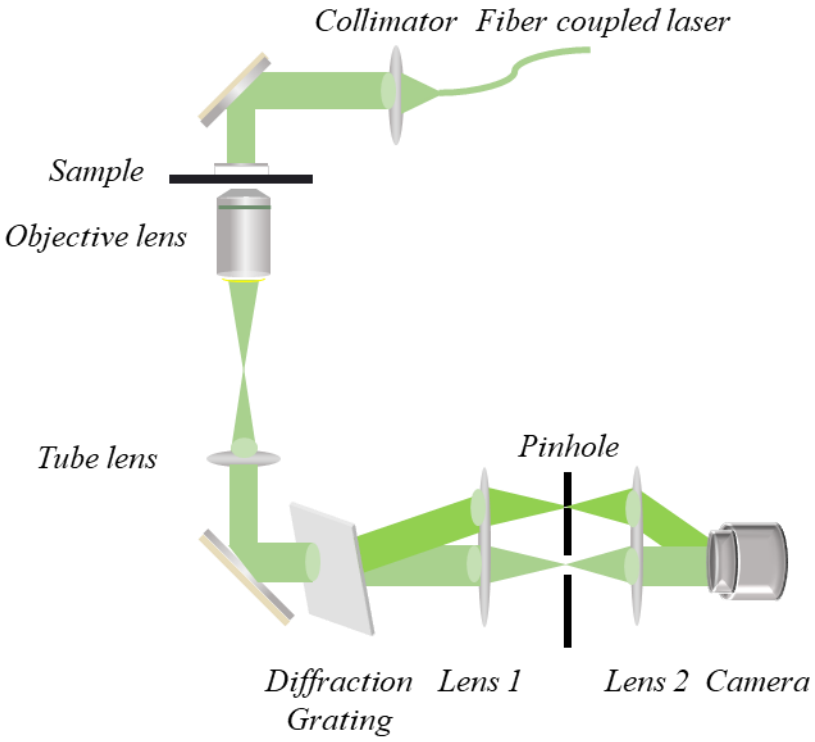

Figure S1. The schematic design of the diffraction phase microscopy system.

Diffraction phase microscopy (DPM) is a common-path quantitative phase microscopy (QPM) method that allows for highly sensitive measurement of cell morphology with nanometer-scale sensitivity.[1] As only one interferogram is needed to obtain a wide-field phase map, high-speed image acquisition is possible with DPM. We have recently developed a portable DPM system with a low-cost to enable a broader adoption.[2] The DPM system, as illustrated in Figure S1, is used to measure the phase maps of the leukocytes. A 532 nm laser (Gem 532, Laser Quantum) is used as the illumination source for the system. The collimated laser beam first passes through the sample, and then the sample scattered field is collected by a water dipping objective lens with numerical aperture (NA) of 1.1 (LUMFLN60XW, Olympus). After that, the sample

beam goes through a tube lens and forms an intermediate image at its back focal plane. A diffraction grating, placed at the intermediate image plane, produces multiple copies of the sample image. Two of the diffraction orders are selected by a subsequential 4*f* system formed by lens 1 and lens 2. The 1st order beam is filtered down to a DC beam (or reference beam) through a 10 μm diameter pinhole filter, placed at the Fourier plane of lens 1. The 0th order beam passes the 4*f* system without any filtering as serves as the signal beam. At the final imaging plane after lens 2, these two beams interfere with each other and form an interferogram which is then captured by a USB camera (FL3-U3-13Y3M-C, Pointgrey). The imaging system has a total magnification of around 100, a lateral resolution of around 590 nm according to the Rayleigh criterion, and a field of view of 61 μm x 49 μm.

2. Quantitative phase image processing

The phase image processing mainly consists of phase retrieval[1] and segmentation, as shown in Figure S2. A Fourier transform is first performed over the raw interferogram (first column in Figure S2), and then a bandpass filter is used to select the +1 or -1 order signal. After that, the selected signal is shifted back to the origin of the frequency spectrum. An inverse Fourier transform is performed to obtain the complex sample field. Meanwhile, another interferogram taken in the sample-free region is used as the calibration image and the same processing is conducted to obtain the complex calibration field. Then the calibration complex field is divided from the sample complex field to obtain the calibrated sample field, from which the sample phase map is obtained. Subsequently, a phase unwrapping procedure is added to unwrap the sample phase map. Finally, we flatten and zero the phase map by removing the background tilt and subtracting the background phase value. Representative phase images for each major leukocyte type are shown in the second column in Figure S2. After obtaining the phase images, we select each individual cells with a segmentation algorithm[3] and create cell phase maps (third column in Figure S2). To ensure the same size for all the cell phase maps, we paste each cell phase map on a fixed-size template.

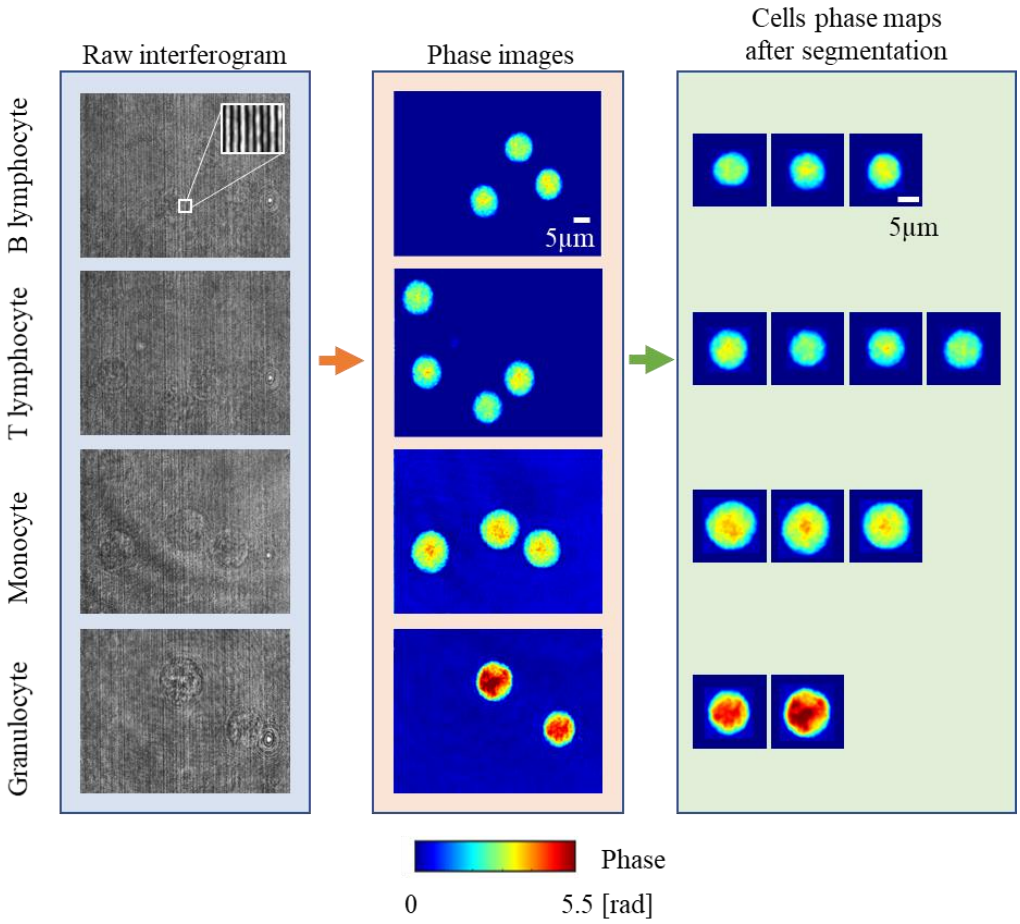

Figure S2. Illustration of the quantitative phase image processing steps. The phase retrieval step is first performed over the raw interferograms (representative interferograms for each major leukocyte type are shown) to obtain the phase images. In the second step, a segmentation algorithm is used to select individual cells and create their phase maps.

3. Comparison between the single-step classifier and the cascaded classifier

Table S1. Comparison between single-step classifier and cascaded classifier on donor 2				
Experiment	B cell (F1-score)	T cell (F1-score)	Monocyte (F1-score)	Granulocyte (F1-score)
Single-step classifier	81.3%	78.8%	88.8%	92.8%
Cascaded classifier	80.9%	81.2%	90.2%	92.5%
Table S2. Comparison between single-step classifier and cascaded classifier on donor 3				
Experiment	B cell (F1-score)	T cell (F1-score)	Monocyte (F1-score)	Granulocyte (F1-score)
Single-step Classifier	74.7%	56.4%	87.0%	83.7%
Cascaded classifier	75.3%	68.5%	94.5%	96.0%

4. Detailed leukocyte classification results

Table S3. Classification result from the monocyte-granulocyte-lymphocyte classifier

	Predicted type				Recall	F1-score
Label type		Lymphocyte	Monocyte	Granulocyte		
	Lymphocyte	197	2	1	98.5%	97.7%
	Monocyte	4	95	1	95.0%	94.0%
	Granulocyte	2	5	93	93.0%	95.4%
Precision		97.0%	93.1%	97.9%	Accuracy	96.3%

Table S4. Classification result from the B-T lymphocyte classifier

	Predicted type			Recall	F1-score
Label type		B lymphocyte	T lymphocyte		
	B lymphocyte	86	14	86.0%	88.2%
	T lymphocyte	9	91	91.0%	88.8%
Precision		90.5%	86.7%	Accuracy	88.5%

Table S5. Summarized classification result from the cascaded-ResNet

	Predicted type					Recall	F1-score
Label type		B lymphocyte	T lymphocyte	Monocyte	Granulocyte		
	B lymphocyte	86	14	0	0	86.0%	88.2%
	T lymphocyte	9	88	2	1	88.0%	84.6%
	Monocyte	0	4	95	1	95.0%	94.0%
	Granulocyte	0	2	5	93	93.0%	95.4%
Precision		90.5%	81.5%	93.1%	97.9%	Accuracy	90.5%

Table S6. Classification result from the CD4-CD8 classifier from one donor

	Predicted type			Recall	F1-score
Label type		CD4	CD8		
	CD4	37	6	86.0%	80.4%

	CD8	12	31	72.1%	77.5%
Precision		75.5%	83.8%	Accuracy	79.1%

5. Principal component analysis (PCA)

We first reshaped each image with size of 300x300 into a 1x90000 sequence and then used the principal component analysis (PCA)[4] method to decrease the dimension from 90000 to 256. At last, by using the t-distributed stochastic neighbor embedding (t-SNE) method,[5] we visualized the PCA extracted features in the 3-D plot.

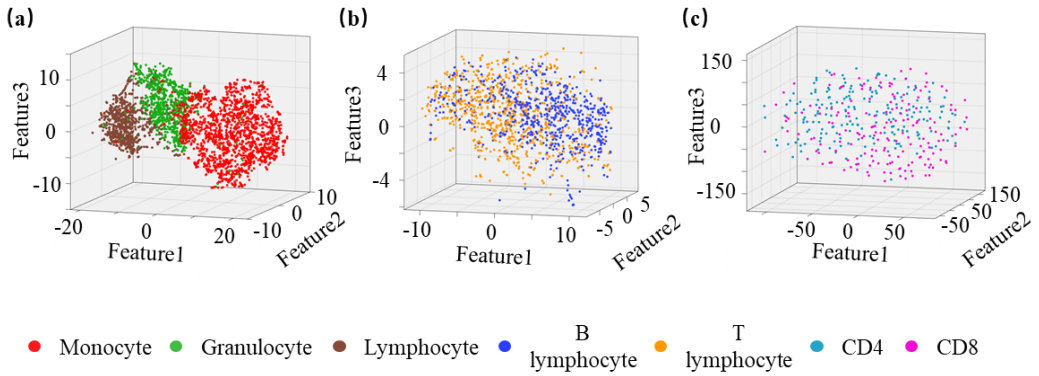

Figure S3. Visualization of the features extracted by PCA using the T-SNE method. a, Visualization of PCA features of monocytes, granulocytes, and lymphocytes. **b**, Visualization of PCA features of B and T lymphocytes. **c**, Visualization of PCA features of CD4 and CD8 cells.

To evaluate the differentiation capability of PCA, we used a support vector machine (SVM) to analyze the features extracted by PCA. We compare the differentiation accuracy between PCA and our neural network model with results presented in Table S7.

Table S7. Classification accuracy comparison between PCA and neural network

Experiment	B lymphocyte (F1-score)	T lymphocyte (F1-score)	Monocyte (F1-score)	Granulocyte (F1-score)
PCA	70.1%	68.2%	89.8%	91.5%
Neural Network	88.2%	84.6%	94.0%	95.4%

6. Neural network layer visualization

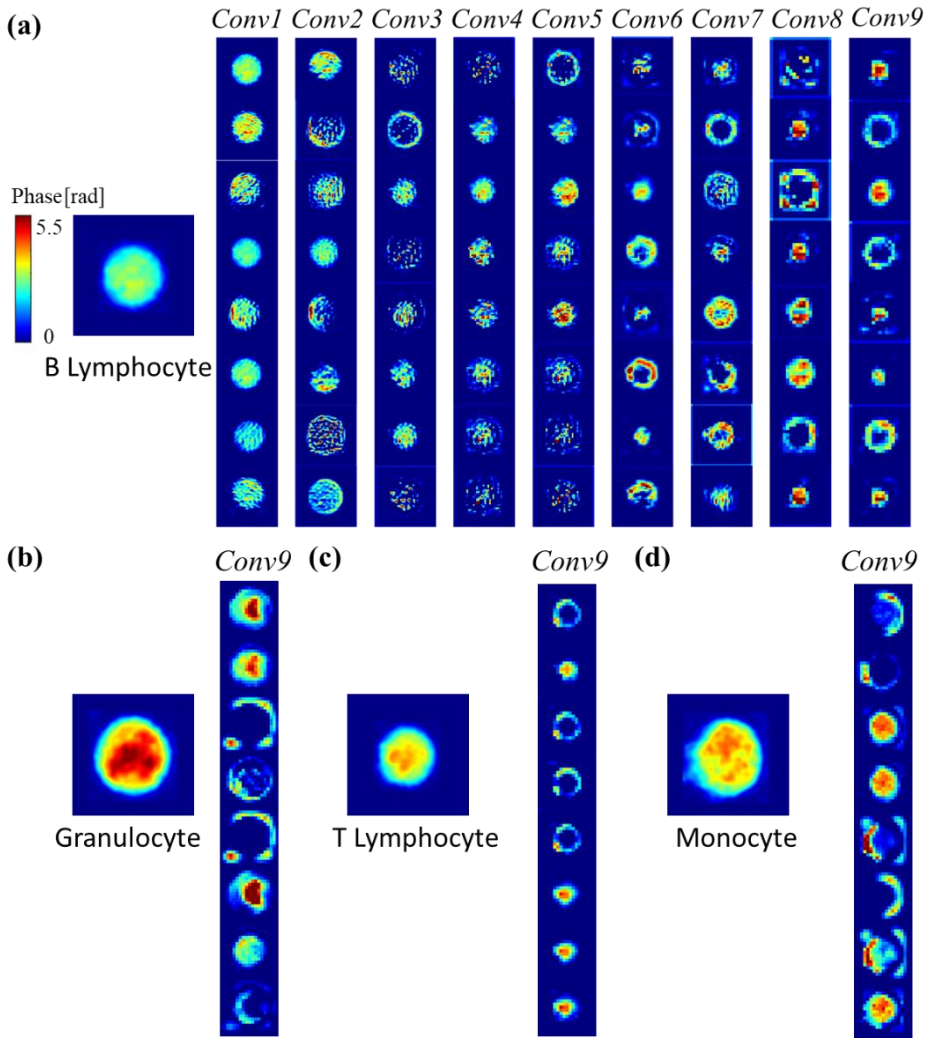

Figure S4. Visualization of the outputs from neural network layers. a, Neural network outputs from each convolutional layer for a B lymphocyte. **b**, Neural network outputs from the last convolutional layer for a granulocyte. **c**, Neural network outputs from the last convolutional layer for a T lymphocyte. **d**, Neural network outputs from the last convolutional layer for a monocyte.

7. Examples of misclassified leukocytes

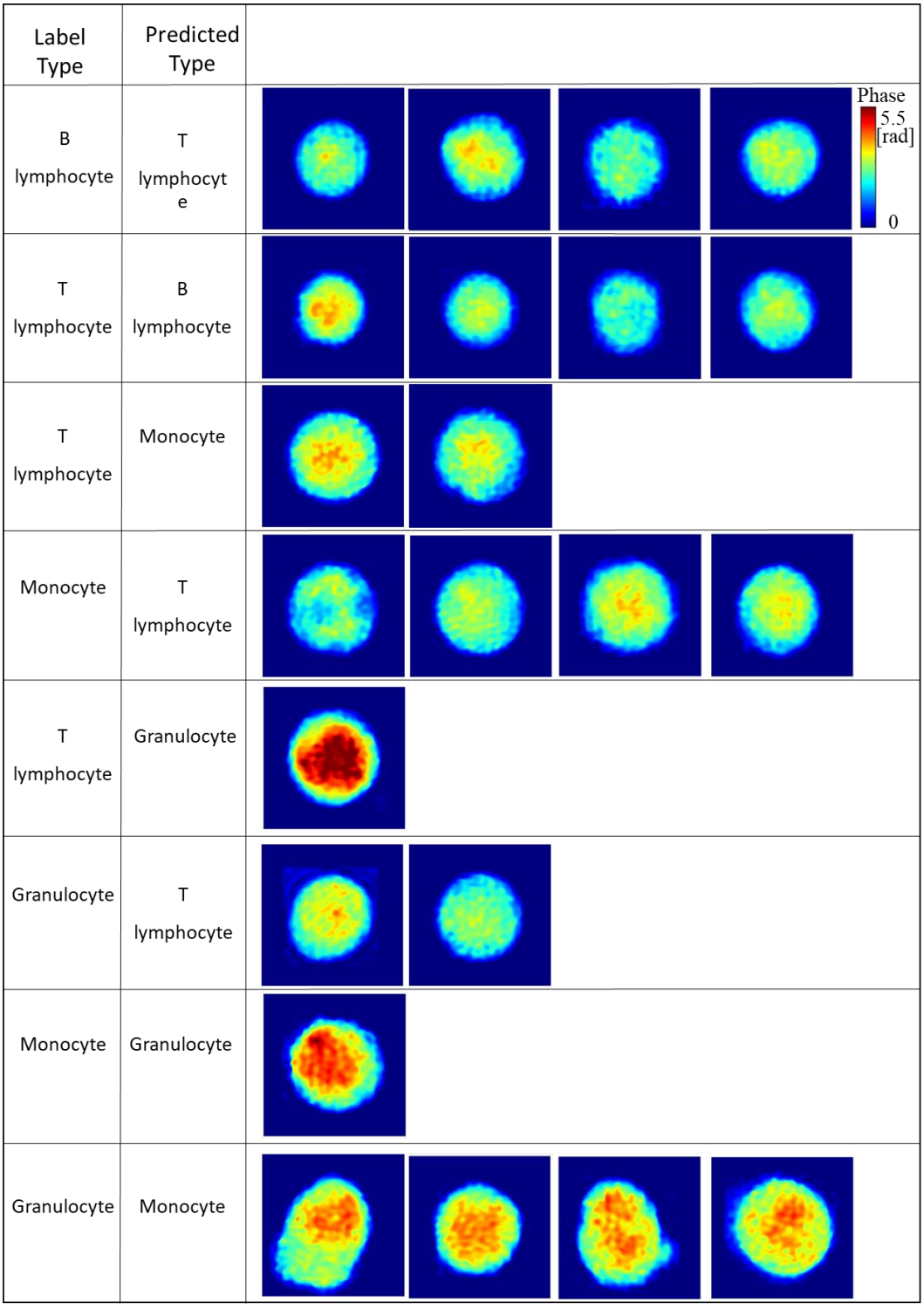

Figure S5. Selected examples of misclassified leukocytes.

To explore the cause of the misclassification, we show the phase maps of several selected misclassified leukocytes and their corresponding actual types and predicted types (Figure S5). We suspect some of the misclassifications might be induced by

mislabeling. For example, the leukocyte labeled as a T lymphocyte but predicted as a granulocyte has large phase values and a large area, which are not in accordance with typical features of T lymphocytes.

8. Training set scale

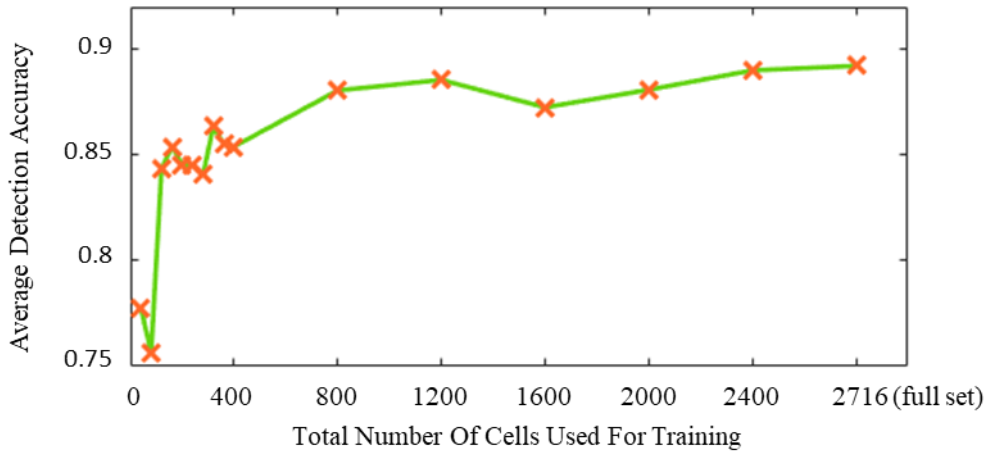

Figure S6. Average detection accuracy vs. total number of cells used for training. Each experiment was repeated 5 times to obtain the average detection accuracy.

9. Detailed cross-donor classification results

Table S8. Cross-donor testing result with cascaded-ResNet

Test donor	B lymphocyte (F1-score)	T lymphocyte (F1-score)	Monocyte (F1-score)	Granulocyte (F1-score)
1	N/A	82.5%	94.4%	97.5%
2	80.9%	81.2%	90.2%	92.5%
3	75.3%	68.5%	94.5%	96.0%
4	N/A	81.3%	87.8%	90.9%
5	94.9%	N/A	N/A	N/A
6	N/A	93.5%	91.3%	94.6%
Average	83.7%	81.4%	91.6%	94.3%

*N/A represents when such data is unavailable, or the dataset is too small to have a statistical significance.

Table S9. Cross-donor testing result from the monocyte-granulocyte-lymphocyte classifier

Test donor	Lymphocyte (F1-score)	Monocyte (F1-score)	Granulocyte (F1-score)

1	96.8%	94.4%	97.5%
2	98.2%	90.2%	92.5%
3	97.4%	94.5%	96.0%
4	90.0%	87.8%	90.9%
5	99.9%	N/A	N/A
6	96.0%	91.3%	94.6%
Average	96.4%	91.6%	94.3%
*N/A represents when such data is unavailable, or the dataset is too small to have a statistical significance.			

Table S10. Cross-donor testing result from the B-T lymphocyte classifier

Test donor	B lymphocyte (F1-score)	T lymphocyte (F1-score)
1	N/A	85.5%
2	81.7%	82.9%
3	75.9%	71.5%
4	N/A	92.0%
5	94.9%	N/A
6	N/A	97.6%
Average	84.1%	85.9%
*N/A represents when such data is unavailable, or the dataset is too small to have a statistical significance.		

10. Intra-donor analysis

In each intra-donor analysis test, the testing set consisted of 30 cells per type that were randomly chosen from each type. The rest (>70 cells per type) were used to train the ResNet-10 classifier. The result is summarized below:

Table S11. Intra-donor testing result

Test donor	B lymphocyte (F1-score)	T lymphocyte (F1-score)	Monocyte (F1-score)	Granulocyte (F1-score)
1	N/A	100%	100%	100%
2	90.3%	93.1%	93.5%	96.6%
3	76.1%	68.0%	96.7%	98.3%
4	N/A	88.1%	85.7%	96.6%
5	N/A	N/A	N/A	N/A

6	N/A	96.7%	93.3%	96.7%
Average	83.2%	89.2%	93.8%	97.6%
*N/A represents when such data is unavailable, or the dataset is too small to have a statistical significance.				

11. Flow cytometry measurements

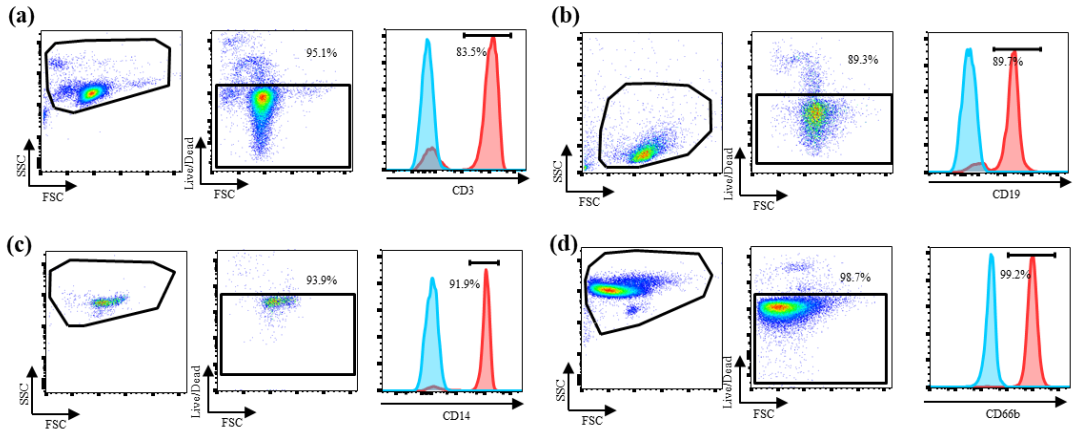

Figure S7. Flow cytometry analysis for the purity of isolated leukocytes showing the polygonal gating for live leukocytes along with the fluorophore-conjugated antibodies for each leukocyte type. a, Anti-CD3-PE for T lymphocytes. **b**, Anti-CD-19-APC for B lymphocytes. **c**, Anti-CD-14-PerCP for monocytes. **d**, Anti-CD-66b-FITC for granulocytes. FSC: forward scatter; SSC: side scatter.

The flow cytometry results for assessing the purity of isolated leukocytes are illustrated in Figure S7. The percentage population for T lymphocytes, B lymphocytes, monocytes, and granulocytes in representative isolated leukocyte samples were 83.5%, 89.7%, 91.9%, and 99.2%, respectively.

12. Comparison with results from existing methods

Table S12. Comparison of AIRFIHA with existing methods on classification accuracy (F1-score)

Method	Labeling method	Sample type	Cross-validation	Result				
				Monocyte	**Granulocyte**	**Lymphocyte**		
Bright and dark field microscope[6]	Fluorescence cytometry	Human	Yes	96.0%	96.4% (Neutrophil) 96.3% (Eosinophil)	96.9%		
Lens-free holography[7]	Fluorescence cytometry	Human	No	98.4%	98.5%	98.7%		
Lens-free holography[8]	Negative Immunomagnetic depletion	Human	No	91.0%	92.8%	85.5%		
Third harmonic generation microscope[9]	Density centrifugation + Scattered light cytometry + Negative fluorescence cytometry	Human	No	97.5%	97.5%	98.0%		
AIRFIHA	Negative Immunomagnetic depletion	Human	No	94.0%	95.4%	97.7%		
AIRFIHA	Negative Immunomagnetic depletion	Human	Yes	91.6%	94.3%	96.4%		
						B lymphocyte	**T lymphocyte**	
Bright and dark field microscope[6]	Fluorescence cytometry	Human	Yes			79.4%	75.7%	
Optical diffraction tomography[10]	Fluorescence cytometry	Mice	No			88.4%	90.9%	
AIRFIHA	Negative Immunomagnetic depletion	Human	No			88.2%	88.8%	
AIRFIHA	Negative Immunomagnetic depletion	Human	Yes			84.1%	85.9%	
							CD4	**CD8**
Optical diffraction tomography[10]	Fluorescence cytometry	Mice	No				85.7 %	88.8 %
AIRFIHA	Negative Immunomagnetic depletion	Human	No				80.4 %	77.5 %

References

[1] B. Bhaduri, C. Edwards, H. Pham, R. Zhou, T. H. Nguyen, L. L. Goddard, G. Popescu, Adv. Opt. Photonics **2014**, 6, 57.

[2] M. Niu, G. Luo, X. Shu, F. Qu, S. Zhou, Y. Ho, N. Zhao, R. Zhou, Photonics Res. **2020**, 8, 1253.

[3] D. Jin, Y. Sung, N. Lue, Y.-H. Kim, P. T. So, Z. Yaqoob, Cytom. A **2017**, 91, 450.

[4] H. Hotelling, Journal of educational psychology **1933**, 24, 417.

[5] L. v. d. Maaten, G. Hinton, J. Mach. Learn. Res. **2008**, 9, 2579.

[6] M. Nassar, M. Doan, A. Filby, O. Wolkenhauer, D. K. Fogg, J. Piasecka, C. A. Thornton, A. E. Carpenter, H. D. Summers, P. Rees, H. Hennig, Cytom. A **2019**, 95, 836.

[7] Y. Li, B. Cornelis, A. Dusa, G. Vanmeerbeeck, D. Vercruysse, E. Sohn, K. Blaszkiewicz, D. Prodanov, P. Schelkens, L. Lagae, Comput. Biol. Med. **2018**, 96, 147.

[8] M. Ugele, M. Weniger, M. Stanzel, M. Bassler, S. W. Krause, O. Friedrich, O. Hayden, L. Richter, Adv. Sci. **2018**, 5, 1800761.

[9] C. H. Wu, T. D. Wang, C. H. Hsieh, S. H. Huang, J. W. Lin, S. C. Hsu, H. T. Wu, Y. M. Wu, T. M. Liu, Sci. Rep. **2016**, 6, 37210.

[10] J. Yoon, Y. Jo, M.-h. Kim, K. Kim, S. Lee, S.-J. Kang, Y. Park, Sci. Rep. **2017**, 7, 6654.